Hypoxia determines survival outcomes of bacterial infection through HIF-1alpha dependent re-programming of leukocyte metabolism

One Sentence Summary: Hypoxia reprograms the innate response to bacterial infection with consequence for host survival.

Authors: A.A.R. Thompson[1†], R.S. Dickinson[2†], F. Murphy[2], J. P. Thomson[3], H.M. Marriott[1], A. Tavares[4], J. Willson[2], L. Williams[1], A. Lewis[1], A. Mirchandani[2], P. Dos Santos Coelho[2], C. Doherty[2], E. Ryan[2], E. Watts[2], N. M. Morton[4], S. Forbes[4], R. H. Stimson[4], A. G. Hameed[1], N. Arnold[1], J.A. Preston[1], A. Lawrie[1], V. Finisguerra[5,6], M. Mazzone[5,6], P. Sadiku[2], J. Goveia[7,8], F. Taverna[7,8], P. Carmeliet[7,8], S.J. Foster[9], E.R. Chilvers[10], A.S. Cowburn[10,11], D.H. Dockrell[1], R.S. Johnson[11], R. R. Meehan[3], M.K.B. Whyte[2], S.R. Walmsley[2*]

Affiliations: [1]Department of Infection, Immunity and Cardiovascular Disease, University of Sheffield, Sheffield, UK. [2]MRC/University of Edinburgh Centre for Inflammation Research, Queen's Medical Research Institute, University of Edinburgh, Edinburgh, UK. [3]MRC Human Genetics Unit at the Institute of Genetics and Molecular Medicine at the University of Edinburgh, Edinburgh, UK. [4]University of Edinburgh/BHF Centre for Cardiovascular Science, Queen's Medical Research Institute, University of Edinburgh, Edinburgh, UK. [5]Laboratory of Molecular Oncology and Angiogenesis, Vesalius Research Center, VIB, Leuven, B3000, Belgium. [6]Laboratory of Molecular Oncology and Angiogenesis, Vesalius Research Center, Department of Oncology, KU Leuven, Leuven, B3000, Belgium. [7]Laboratory of Angiogenesis and Vascular Metabolism, Vesalius Research Centre, VIB, Leuven, B3000, Belgium. [8]Laboratory of Angiogenesis and Vascular Metabolism, Vesalius Research Centre, K.U. Leuven, B3000, Belgium. [9]Department of Molecular Biology and Biotechnology, University of Sheffield, Sheffield, UK. [10]Department of Medicine, University of Cambridge, Cambridge, UK.[11]Department of Physiology, Development and Neuroscience, University of Cambridge, UK. *Correspondence to:

sarah.walmsley@ed.ac.uk †Joint first author

This is a peer-reviewed, accepted author manuscript of the following research article:
Thompson, A. A. R., et. al., Hypoxia determines survival outcomes of bacterial infection through HIF-1α–dependent reprogramming of leukocyte metabolism. Science Immunology, 2(8), https://doi.org/10.1126/sciimmunol.aal2861

Abstract:

Hypoxia and bacterial infection frequently co-exist, in both acute and chronic clinical settings, and typically result in adverse clinical outcomes. To ameliorate this morbidity, we investigated the interaction between hypoxia and the host response. In the context of acute hypoxia, both *S. aureus* and *S. pneumoniae* infections rapidly induced progressive neutrophil mediated morbidity and mortality, with associated hypothermia and cardiovascular compromise. Preconditioning animals through longer exposures to hypoxia, prior to infection, prevented these pathophysiological responses and profoundly dampened the transcriptome of circulating leukocytes. Specifically, perturbation of HIF pathway and glycolysis genes by hypoxic preconditioning was associated with reduced leukocyte glucose utilisation, resulting in systemic rescue from a global negative energy state and myocardial protection. Thus we demonstrate that hypoxia preconditions the innate immune response and determines survival outcomes following bacterial infection through suppression of HIF-1α and neutrophil metabolism. The therapeutic implications of this work are that in the context of systemic or tissue hypoxia therapies that target the host response could improve infection associated morbidity and mortality.

Introduction

A close and bi-directional relationship between hypoxia and inflammation is well recognised. Hypoxia can induce inflammation, for example in acute mountain sickness, and inflamed tissues are typically hypoxic, in part due to oxygen consumption by inflammatory cells (*1*). Localised hypoxia is also a feature of tissues infected with a range of different pathogens (*2, 3*). Systemic hypoxia (hypoxemia) is a clinical characteristic of acute conditions, such as adult respiratory distress syndrome (ARDS) (*4*), and of chronic diseases such as COPD (*5*) but how hypoxemia modifies host responses to infection is largely unknown.

Results

Acute hypoxia induces rapidly progressive morbidity following local infection with *Staphylococcus aureus*.

Staphylococcus aureus, an important human pathogen, is commonly found in critical care settings (*6*) where patients can be profoundly hypoxemic. Host responses to *S. aureus* infection depend critically upon the presence and functionality of myeloid cells, both in animals (*7, 8*) and humans (*9*). We used a model of subcutaneous *S. aureus* infection to investigate the effects of systemic hypoxia on outcomes of infection. Subcutaneous *S. aureus* (SH1000 strain) produced a macroscopic skin lesion in normoxic mice, which developed over 7 days and was well-tolerated (fig. S1, A to C). The same bacterial challenge in the setting of acute hypoxia (10% FiO_2), however, caused significant and progressive

sickness behaviour and hypothermia (Fig.1, A, B, fig. S1, D, E). These responses were accompanied by bradycardia (Fig.1, C), hypotension (Fig.1, D), and impaired cardiac function, with reduced cardiac ejection fraction (Fig.1, E) and cardiac index (Fig.1, F, fig. S1, F) ultimately leading to death. Hypoxia-induced hypothermic responses to subcutaneous *S. aureus* were also observed with heat killed SH1000 (fig. S2, A), and replicated by intra-peritoneal administration of bacterial lipopolysaccharide (LPS) (fig. S2, B). Additional validation of the sickness phenotype was provided by radiotelemetry (fig. S2, C-F). The phenotype was confirmed in an outbred mouse strain (fig. S2, G) and independent of whether infection was during daytime or night-time (fig. S2, H, I). A graded phenotypic response was observed over a range of oxygen tensions 21-10% O_2 (Fig.1, G, H). Importantly, this pathophysiological response occurred in the context of equivalent myeloid cell recruitment (fig. S3, A-C) and bacterial burden (fig. S3, D) with no evidence of *S. aureus* extravasation into the blood or seeding to kidneys, liver or spleen.

In keeping with the observed morbidity, higher serum corticosterone and creatinine (fig. S4, A, B) levels were detected in hypoxia-exposed mice. A full SIRS response was not observed, however, with plasma cytokines either below the limits of detection (IL-1β, TNFα, IFNγ, IL-10, IL-4, IL-13 and IL-22) or unchanged between hypoxic and normoxic mice (fig. S4, C-E), as were levels of the matrix metalloproteinase MMP9 (fig. S4, F), plasma nitrates ($NO_{(X)}$) (fig. S4, G) and malondialdehyde (MDA), a marker of oxidative stress (fig. S4, H). The presence of nitrosylated tyrosine oxidative products in the skin was also

unaffected (fig. S4, I, J). Gross organ function was preserved under hypoxia with equivalent peripheral blood leukocyte profiles (marrow) (fig. S5 A), and normal serum aspartate transaminase (AST) (liver) and lipase (pancreas); circulating metabolic and stress responses (lactate, ATP, PGE_2 and catecholamine levels) were also equivalent (fig. S5, B-H). There was no evidence of cerebrovascular leak, with undetectable levels of Evans blue dye in the brain tissue, and no evidence of lung injury, with equivalent wet-dry lung weight ratios, alveolar cell counts and lung architecture (fig. S6, A-D).

Increased mortality is observed following systemic infection with *Streptococcus pneumoniae* in the setting of acute hypoxia.

To define whether the morbidity observed with *S. aureus* in hypoxia was restricted to that organism or specific to the skin, where low oxygen tensions are reported in health (*10, 11*), we extended our experiments to a model of bacteremic pneumonia (*12*). In keeping with the *S. aureus* phenotype, challenge with intratracheal high-dose serotype 2 *S. pneumoniae* in the context of acute hypoxia resulted in increased sickness responses and associated hypothermia (Fig.1, I, J). This was again independent of bacterial burden, with equivalent lung CFU counts at 14 and 24h (Fig.1, K) and blood CFU counts lower at 14h and equivalent at 24h (Fig.1, L) when comparing hypoxic and normoxic animals. Reduced numbers of neutrophils and macrophages were recruited to the airways at 14h in hypoxia-exposed mice but cell counts were equivalent to normoxic mice

by 24h (Fig.1, M-O) and no differences in IgM levels, a marker of lung injury, were observed (Fig.1, P). Importantly, when infection was allowed to progress beyond 24h, approximately half of normoxic mice cleared the infection, while all hypoxia-exposed mice died (Fig.1, Q). Thus, at two different sites (skin and lung) and with two different pathogens (*S. aureus* and *S. pneumoniae*), combining infection with acute systemic hypoxia resulted in severe morbidity and later fatality, which occurred despite equivalent control of bacterial infection and absence of a typical SIRS response, oxidative damage or multi-organ failure.

Hypoxic preconditioning prior to infection protects against the increase in morbidity and mortality observed with acute hypoxia.

These profound acute physiological consequences of combined hypoxia and infection parallel human observations in the critical care setting, where increased mortality is described in hypoxemic patients who present with or develop bacterial infections (*6, 13, 14*). The clinical situation for chronic hypoxia is more complex. In COPD, for example, infective exacerbations and hypoxemia are each independently associated with disease progression (*15, 16*), yet bacteria are frequently present in the airways of clinically stable hypoxemic patients without severe systemic compromise (*17*). We therefore questioned whether more prolonged hypoxia could modify the systemic response to infection. Mice preconditioned for 7 days at 10% O_2 prior to *S. aureus* infection showed marked protection from the acute hypoxia-associated systemic phenotype (Fig. 2, A, B).

Importantly, hypoxic preconditioning also reversed sickness and hypothermic responses and mortality observed with intra-tracheal administration of *S. pneumoniae* (Fig. 2, C-E). Hence preconditioning confers this protection following challenge by different bacterial pathogens, with different sites of infection, and in both localised and disseminated bacterial infections.

Hypoxic preconditioning rescues the host from a global negative energy state.

At a cellular level, adaptation to hypoxia critically depends upon co-ordinated metabolic responses that both maintain ATP production and modify energy requirements. The consequences of hypoxia and hypoxic preconditioning on metabolism were therefore explored. Indirect calorimetry revealed that animals infected in the setting of acute hypoxia preferentially switched towards carbohydrate utilisation in contrast to normoxia where fat and carbohydrates were proportionately consumed (Fig. 2, F). In keeping with the suggestion of an increased reliance on glycolysis, hypoxic mice displayed a significant loss of liver glycogen (Fig. 2, G). Infection combined with acute hypoxia resulted in a negative energy state with loss of inguinal (white) and intrascapular (brown) adipose tissue (Fig. 2, H, I), increased serum ketone production (Fig.2, J) and lower circulating glucose levels in animals that succumbed to infection (Fig. 2, K). Hypoxic preconditioning rescued the animals from this negative energy state, with restoration of proportionate fat and carbohydrate consumption, liver

glycogen reserves and fat mass, reduction in circulating ketones and restoration of circulating fasting glucose and insulin levels (Fig. 2, F-M). Furthermore, whilst brown fat glucose uptake was suppressed (Fig. 2, N), in vivo ^{18}F-FDG PET studies identified enhanced glucose uptake by the myocardium following preconditioning (Fig. 2, O, P, fig. S7, A), with a parallel increase in cardiac function observed by measures of cardiac index and ejection fraction (Fig. 2, Q,R).

Hypoxic preconditioning responses are retained in the circulating leukocyte population, with morbidity a neutrophil mediated response.

To determine the longevity of the preconditioning response, mice experienced 1 week of hypoxia before being maintained in normoxia for up to 28 days prior to bacterial challenge in hypoxia. Protection was maintained even after 7 or 28 days of normoxic re-acclimatisation (Fig. 3, A-D). Thus, the marked protection observed with hypoxic preconditioning extends significantly beyond the initial period of exposure.

The importance of leukocyte populations in regulating outcomes following hypoxic preconditioning was explored in a series of bone marrow transfer experiments. Importantly, reconstitution of hypoxia-naïve mice with hypoxia preconditioned bone marrow, following fractional radiation (*18, 19*) to ensure selective targeting of the marrow population, conveyed protection from the morbidity (Fig. 3, E, F, fig. S7, B-D) and mortality observed in both infection

model systems (Fig. 3, G). These results implicate circulating leukocyte populations both in driving the systemic phenotypes observed in acute hypoxia and in rescuing this response following hypoxic preconditioning. Anti-Ly6G (neutrophil) and clodronate (mononuclear cells) depletion (fig. S7, E) subsequently identified the hypoxia induced hypothermic responses to be neutrophil-dependent (Fig. 3, H). To address the mechanism by which preconditioning reprograms neutrophil glucose utilisation and protects against cardiac decompensation, we undertook RNA sequencing of circulating leukocytes following acute hypoxia in the presence or absence of infection with *S. pneumoniae* and of hypoxic preconditioning. Whilst global transcriptional states were largely unaltered between the four conditions (mean Pearson correlation score 0.88), a number of genes displayed strong expression changes, with the majority of changes a hallmark of preconditioning alone (Fig.3, I-K).

Preconditioning represses leukocyte HIF pathway and glycolysis genes resulting in suppression of glucose utilisation and phenotypic rescue.

Pathway analysis revealed unique signatures between the treatment groups (fig. S8), with suppression of HIF-1α pathway genes by preconditioning (fig. S9, A-C) further validated at both an RNA (Fig. 4, A, B) and protein level (Fig. 4, C). HIF-1α is widely recognised to play a central role in co-ordinating cellular adaptive responses to hypoxia (*20*), including energy metabolism, and in regulating myeloid cell phenotypes (*19, 21-24*). Correlative heatmap analysis and

hierarchical clustering of the subset of 1,274 detected metabolic genes revealed distinct metabolic gene expression signatures between preconditioned and naïve states (Fig. 4, D). Metabolic pathway analysis subsequently detailed the relative suppression of glucose transporters and key unidirectional glycolytic enzymes, validated by quantitative PCR (Fig. 4, E, fig. S9, D-F) and western blot (Fig. 4,C). A reduction in glycolysis following preconditioning was subsequently demonstrated by suppression of extracellular acidification rates (Fig. 4, F), with diminished glucose uptake by circulating and recruited leukocytes confirmed in vivo by ^{18}F-FDG PET studies (Fig. 4, G, H). Finally, to validate leukocyte HIF-1α expression as the critical mediator of systemic morbidity, HIF-1α (*Hif1a*$^{flox/flox}$;*LysMcre*$^{+/-}$) deficient mice were challenged with *S. aureus.* Myeloid specific loss of HIF-1α (*Hif1a*$^{flox/flox}$;*LysMcre*$^{+/-}$), independent of effects either on local bacterial counts or systemic cytokine release (fig. S10, A-D), conveyed near-complete protection from the heightened sickness responses and hypothermia in hypoxia-exposed mice (Fig.4, I, J). This protection was equivalent to the effect of preconditioning alone (fig. S10, E). Administration of a non-selective pan hydroxylase inhibitor (DMOG) was unable to supress leukocyte HIF expression and therefore did not confer protection in this model system (fig. S10, F-H). In keeping with metabolic protection, mice with myeloid-specific targeted deletions of HIF-1α (*Hif1a*$^{flox/flox}$;*LysMcre*$^{+/-}$) displayed higher circulating glucose levels following infection, even in the non-fasting state (Fig.4, K).

Discussion

A significant body of work employing conditional knockout mice has developed our understanding of how the HIF hydroxylase pathway modifies myeloid cell function and survival. Studies have delineated context specific roles for individual family members in the regulation of macrophage invasion and motility (*21*), macrophage bacterial killing (*21, 22*) and neutrophil survival (*19, 23, 25*) and phagocytosis (*26*), both in the setting of regional hypoxia and following bacterial infection. The consequences of systemic hypoxia and bacterial infection acting in concert have not previously been examined in detail but are highly relevant to clinical situations, given the co-existence of systemic hypoxia and bacterial infection in e.g. the Adult Respiratory Distress Syndrome (ARDS) and of systemic hypoxia and bacterial colonisation of the airways in chronic obstructive pulmonary disease (COPD).

Our studies in murine models of both localised and systemic acute infection in the setting of acute hypoxaemia, demonstrate the catastrophic in vivo consequences of exaggerated leukocyte HIF-1α activation. Profound pathophysiological responses occur as a consequence of an imbalance in glucose availability and utilisation, with animals infected in the setting of acute hypoxia demonstrating a skewing toward carbohydrate utilisation, loss of liver glycogen stores, consumption of white and brown adipose tissue, elevated ketone production, and the eventual development of a circulating hypoglycaemia. Strikingly animals show preserved bacterial killing capacity despite metabolic compromise. The equivalence of bacterial burden under each oxygen tension

studied together with the divergence between bacterial clearance and overall morbidity and mortality, thus indicate the importance of targeting the host response, in combination with an anti-microbial strategy to improve outcomes where hypoxia and infection co-exist.

Hypoxia and infection can exist chronically e.g. in chronic obstructive pulmonary disease (COPD). Experimental modelling of a more chronic state of hypoxia and bacterial infection showed we could ameliorate the observed increase in morbidity and mortality by prior exposure of animals to hypoxia. This protection extended beyond the initial hypoxic exposure period, was sustained over time and both dependent upon and retained by the bone marrow compartment. These data suggest that hypoxic preconditioning changes bone marrow leukocyte populations which, when released into the circulation following bacterial challenge, demonstrate altered behaviours that in turn determine the host outcome. Subsequent phenotypic rescue with anti-Ly6G depletion demonstrated the hypothermic and sickness responses were neutrophil mediated. Thus, short lived circulating cells can possess functional memory of previous hypoxic challenges resulting in modified innate immune responses. Whilst HIF-1α dependent training of responses to bacterial sepsis and a fungal cell wall component has been observed (*27*), our work provides the first evidence that oxygen availability is a critical determinant of morbidity and mortality outcomes following bacterial infection.

Immune cell metabolism can profoundly influence key inflammatory responses. Macrophage polarisation states in part driven by metabolic processes. Both anti-

microbial M1 macrophages and neutrophils depend upon glycolysis, yet tissue repair M2 macrophages require fatty acid oxidation and oxidative phosphorylation for ATP production with the TCA cycle dominating over glycolysis (*28-31*). Neutrophils in contrast demonstrate a disordered TCA cycle even in the resting state (*32*). Consequences of metabolism for immune responses are therefore cell-type specific and will also vary in physiological and patho-physiological disease states. In the models studied, we saw no effect of clodronate mediated mononuclear cell depletion on either hypoxia induced hypothermia or sickness whereas neutrophil depletion protected from the sickness response. We therefore propose that neutrophil dependence upon glucose, whilst a beneficial adaptive response under normal systemic oxygenation, drives a fatal response in the context of systemic hypoxia where global glucose requirements are increased resulting in the development of hypoglycaemia and cardiac failure. There are precedents that cell-type specific metabolic responses can influence the metabolism of other organs with consequences for the host. As examples, skeletal muscle deletion of Phd2 conveys protection from myocardial ischaemia reperfusion injury through the regulation of hepatic kynurenic acid production (*33*), whilst M2 macrophages can co-ordinate browning of subcutaneous white adipose tissue (*34*).

We observed HIF-1α to be the critical mediator of the heightened sickness responses, with myeloid specific loss of HIF-1α conveying protection from hypothermia, sickness and hypoglycaemia following challenge with *S. aureus*. This is of interest, given that HIF-1α deficiency has previously linked to impaired

bacterial killing (*21*) and negative outcomes in more fulminant bacterial models (*22*). Thus, the innate immune response must be exquisitely sensitive to HIF-1α levels of activity, with both insufficient (fulminant infection models) and excessive (acute infection and hypoxia) HIF-1α activation associated with poor outcomes, and hypoxic preconditioning enabling the restoration of this finely tuned response. Understanding the mechanisms that regulate HIF-1α expression, stability and activity will therefore be critical in the development of strategies that target the innate immune response. Whilst stabilisation of HIF-1α protein in innate immune cells is well characterised in the setting of hypoxia, regulation of HIF-activity has also been described following pathogen challenge (*22*), exposure to bacterial lipopolysaccharide cell membrane fraction (*35*) and iron chelation (*36*). More recently small metabolite regulation of HIF-1α stability in both near-haploid cells (*37*) and $CD8^+$ T-lymphocytes (*38*) has been described, with HIF-1 dependent accumulation of S-2-hydroxyglutarate (S-2HG) following T-cell receptor triggering further augmenting HIF signalling in both normoxic and hypoxic culture conditions. A further level of complexity is added with the observation that S-2HG can also inhibit the 2-oxoglutarate-dependent epigenetic modifiers that demethylate histones (Jumonji C containing proteins) or oxidise 5-methylcytosine in DNA (Ten-eleven translocation (Tet) proteins)(*39-41*). Thus in a model of T-cell receptor triggering changes in small metabolite abundance can both regulate HIF-1α expression and lead to alterations in epigenetic marks (*38*). These data combined with the evidence of innate immune training following repeated infectious challenge suggest that further exploration of the links

between individual metabolites, epigenetic changes, hypoxia and regulation of HIF pathway responses will be important in delineating the mechanisms by which hypoxia can re-program the neutrophil transcriptome, a limitation of our current study and an area of ongoing research activity.

In summary we show outcomes of infection are profoundly regulated by neutrophil responses to oxygen and nutrient availability. We identify a mechanism by which hypoxic preconditioning induces sustained changes in leukocyte glucose requirements and utilisation as a consequence of transcriptional suppression of leukocyte HIF-1α responses. This in turn defines survival outcomes following local and systemic bacterial challenge, through a restoration of balance between glucose availability and tissue need and independent of recognised anti-microbial function. Our work highlights the potential therapeutic importance of targeting the host response in combination with anti-microbial strategies when treating bacterial infection in the setting of hypoxia.

Materials and Methods

Study design

The goals of this study were to investigate the effects of ambient hypoxia on host responses to *S. aureus* and *S. pneumoniae* infection. We also determined the mechanisms by which hypoxic pre-conditioning prevented adverse outcomes in these infection models. Pilot experiments were performed to define the number of animals required to detect significant differences in body temperature and sickness score between infected animals exposed to hypoxia and those maintained in normoxia. Vehicle-treated animals were also exposed to hypoxia and assessed alongside infected animals. Other end-points included measurements of bacterial burden, serological and physiological parameters as stated under the sub-headings below. The number of biological replicates for each experimental group are indicated in the figure legends. *In vivo* experiments were performed independently at least twice unless otherwise specified. Clinical assessment of mouse sickness behavior was made by two independent observers blinded to which oxygen tension the mice had been exposed. Study design was approved with authorisation of our project licence in accordance with the Home Office Animals (Scientific Procedures) Act of 1986.

Murine colonies

Lysozyme M-driven cre recombinase (LysMcre) was used to target *Hif1a* (*Hif1a*$^{flox/flox}$;LysMcre$^{+/-}$) deletions in myeloid lineage cells. Animals were back crossed to a C57BL/6 background (*21, 42*). C57BL/6 mice or littermate LysMcre$^{-/-}$

floxed mice were used as controls. All animal experiments were conducted in accordance with the Home Office Animals (Scientific Procedures) Act of 1986 with local ethics approval.

Subcutaneous skin infection model

SH1000, a strain of *S. aureus* derived from the clinical isolate NCTC 8325, was used throughout these experiments (*43, 44*). Mice were injected subcutaneously with live stationary phase bacteria (1×10^7 cfu) before being exposed to hypoxia (10% O_2) or maintained in room air. At indicated time points (6 and 12 hours) mice were assessed alongside normoxic controls. Clinical assessments of mouse sickness behaviour were made and rectal temperature was recorded. Mice were anaesthetised, exsanguinated and tissues processed as described below or in supplementary methods.

Blood pressure and heart rate measurements in awake mice

To obtain readings in awake mice, animals were trained for 7 days to undergo non-invasive blood pressure measurement using a BP-2000 Blood Pressure Analysis System™ (Visitech Systems Inc., Apex, USA). After training, these animals were then injected with either SH1000 bacteria or PBS and exposed to hypoxia or normoxia for 12 hours after which time blood pressure and heart rate measurements were recorded. A minimum of 10 readings were attempted on each animal.

Echocardiography

Twelve hours after subcutaneous injection of bacteria, hypoxic or normoxic mice were anaesthetised with 5% isoflurane supplied in oxygen at 2 l/min and placed on a warming pad. Mice were secured on the pad lying flat and supine. The fur on the chest was clipped and hair removal cream used to ensure good penetration of ultrasound waves. Transthoracic echocardiography was performed by an experienced operator using a VisualSonics Vevo® 770 Imaging system and RMV707B scanhead (VisualSonics, Toronto, Canada).

Bone marrow transplantation

C57BL/6 recipient mice were irradiated with 3 fractions of 1Gy each day for 4 days before injection with $1.5x10^6$ bone marrow cells from C57BL/6 mice exposed to hypoxia (10% O_2) for 7 days or control C57BL/6 mice. *S. aureus* subcutaneous injection experiments were performed 4 weeks following injection of donor marrow, at a time point when tissue macrophages retain a native phenotype.

RNA isolation and relative quantification

Murine peripheral blood leukocytes ($1x10^6$/condition) were lysed and RNA extracted using the mirVana™ total RNA isolation protocols (Ambion, Austin, USA). For RNA quantification, samples were treated with DNase (Ambion) and random hexamer cDNA synthesized by reverse transcription. Assays-on-

demand gene expression TaqMan® MGB 6FAM dye-labeled products (Applied Biosystems) were used for relative quantification of cDNA.

Intratracheal pneumonia model

Wild-type C57BL/6 mice were anaesthetized with ketamine (100mg/kg i.p.; Vetalar V, Pfizer, UK) and acepromazine (5mg/kg i.p.; Calmivet Solution Injectable, Vetoquinol, France). The fur was shaved from the neck and a small incision made. The trachea was then exposed by blunt dissection and cannulated with a 24G cannula (Jelco© radiopaque cannula, Smiths Medical International Ltd. Rossendale, UK). Each mouse then had $1x10^7$ CFU of D39, type 2 *Streptococcus pneumoniae* instilled via the trachea. Control animals were instilled by the same method with PBS. Mice were recovered for 6 hours and then exposed to hypoxia (10% O_2) or maintained in room air. At indicated time points (14 and 24 hours) mice were assessed alongside normoxic controls. Clinical assessment of mouse sickness behaviour was made by two independent observers blinded as to which oxygen tension the mice had been exposed to, and rectal temperature was recorded. Mice were then culled and tissues harvested. For preacclimatisaton experiments, mice were housed in 10% oxygen for 7 days prior bacterial challenge as described above. For the Kaplan-Meier plots, mice were culled once the threshold of sickness was reached.

Assessment of lung injury

Bronchoalveolar lavage was performed via cannulation of the trachea. Total cell counts were calculated using haemocytometer counts and differential counts assessed on cytocentrifugation slides. Levels of IgM and elastase were analyzed using commercially available kits (Mouse IgM ELISA quantitation set, Bethyl Laboratories Inc, Montgomery, USA; EnzChek Elastase Assay Kit, Molecular Probes Europe BV, Leiden, The Netherlands).

Quantification of viable bacterial counts

10-fold serial dilutions were performed on whole blood aliquots. Three 10µl drops from each of 6 dilutions were then plated onto blood agar plates and cultured overnight in 37°C to calculate viable bacterial counts. After collection of the bronchoalveolar lavage fluid, the lungs were carefully dissected and stored in sterile tubes. The lungs were homogenized and 10-fold serial dilutions performed on each sample to calculate viable bacterial counts, which were normalized to count per pair of lungs.

Respiratory exchange ratios

Mice were placed individually into a pre-calibrated home-cage indirect calorimetry Phenomaster system (TSE Systems, GmBH, Bad Homburg, Germany) for 1 hour and oxygen consumption, carbon dioxide production and X-Y-Z activity by infra-red beam breaking were assessed. Flow rate was set to 0.3L/min. Mice cages were sampled for 3 minutes and compared to an empty cage air reference every cycle in 15 minute blocks. RER was calculated from O_2

and CO_2 measurements and the data presented as the average of cycles 2-4 of the one hour period.

Liver histology

Livers were placed in 10% buffered formalin prior to processing and staining with haematoxylin/eosin or Periodic Acid Schiff (PAS) reagents.

Paired plasma biochemical profiling

Animals were fasted for 6 hours prior to sacrifice, and blood collected at end point for glucose, insulin and γ-hydroxybutryate quantification by ELISA (Glucose HK:Sigma, Insulin:Crystal Chem, hydroxbutryate:Sigma, Missouri, USA).

In vivo ^{18}F-FDG-PET

Circulating glucose levels were measured in animals at the time of radiotracer injection. Animals were injected with intra-peritoneal ^{18}F-FDG (5.1±2.2 MBq, 0.2±0.05 mL) 5 and 23 hours following the installation of intra-tracheal *S. pneumonia*. After injection, mice were returned for 1 hour to their original ambient oxygen tensions prior to tissue harvesting for gamma counting or imaging in vivo under isoflurane anesthesia (1.5%, Oxygen 0.5 L/min, Nitrous Oxide 0.5 L/min) using a nanoPET/CT scanner (Mediso Medical Imaging Systems, Hungary). A 30-min whole-body emission scan was obtained using a 1:5 coincidence list mode. At the end of the emission scan, a CT scan was acquired (semi-circular full trajectory, maximum field of view, 480 projections, 55

kVp, 300 ms and 1:4 binning) for attenuation correction and co-registration with PET data. Three-dimensional PET data was reconstructed into 3×10 min frames using Mediso iterative Tera-Tomo 3D reconstruction algorithm and the following settings: 4 iterations and 6 subsets, full detector model, normal regularisation, spike filter on, voxel size 0.6 mm and 400-600 keV energy window. PET data was corrected for randoms, scatter and attenuation. Reconstructed whole-body PET scans were imported into PMOD 3.4 software (PMOD Technologies, Switzerland) and volumes of interest (VOIs) were drawn around organs and tissues of interest. The measured activity of the target organs and tissues was expressed as the standard uptake values (SUV) corrected for circulating glucose levels (SUVglu). Radioactivity levels of collected tissue samples were assessed using an automatic gamma counter (Wizard 1470 Gamma Counter, Perkin Elmer). Measured disintegrations per minute were converted to Becquerel and expressed in percentage injected dose per gram of tissue (%ID/g) and normalized to circulating glucose levels.

Depletion of myeloid cell subsets

Wild-type C57BL/6 mice were injected intraperitoneally with vehicle control, anti-Ly6G antibody (500mg in 500ul per mouse, eBioscience, UK), clodronate or PBS containing liposomes (500ul per mouse, ClodronateLiposomes.com). Twelve hours later, the mice were challenged with subcutaneous SH1000 and housed in either normoxia (21% O_2) or hypoxia (10% O_2). At 12 hours following the challenge, clinical assessment of sickness was performed by two separate

observers and rectal temperature recorded. Mice were then anaesthetised and 200uL of whole blood cell was collected into vials containing 2mM EDTA. Red cells were twice lysed in red cell lysis buffer (Biolegend) and cells were washed in FACS buffer (PBS+2mM EDTA+2%BSA). Cells were stained using Ly6C FITC (Biolegend), Lineage (CD3, CD19 (both Biolegend), Siglec F (BD Biosceinces) PE, CD115 APC (Biolegend), 7-AAD (Biolegend), CD45 AF700 (Biolegend), Ly6G Pacific Blue (Biolegend). Cells were acquired using a BD Fortessa 6 laser flow cytometer.

RNA sequencing and analysis

Murine peripheral blood leukocytes ($1x10^6$/condition) were lysed and RNA extracted using Qiagen mini total RNA isolation protocols (Qiagen, Germany). Samples were treated with DNase (Ambion), and sample integrity verified on the Agilent Bioanalyser with the RNA Nano chip. Illumina Tru-seq paired end strand specific sequencing (Illumina, USA) was carried out on a NextSeq-550 sequencer (Edinburgh Clinical Research Facility, Western General Hospital, Edinburgh, Scotland, UK). 500ng of Total RNA underwent ribosomal RNA depletion (rRNA) prior to purification, fragmentation, random hexamer cDNA generation and purification with AMPure XP beads (Beckman-Coulter, USA). Multiple indexing adapters were ligated to ds cDNA with subsequent hybridisation onto flow cells, and DNA fragment enrichment by 15 cycle PCR for sequencing. Completed libraries were quantified by qPCR using the KAPA Illumina Library Quantification Kit (Illumina, USA) before multiplexing in two

equimolar pools and running on two flow cells on the Illumina NextSeq 550. The resulting FastQ files were mapped to the reference genome (mm9) using the Tophat alignment tool (V1) on Illumina Basespace software and reads per kilobase per million (RPKM) scores calculated. Differentially expressed genes were identified using Cufflinks and the Differential expression tool on the Illumina Basespace software. Genes showing greater than 2 fold change with Deseq generated P-values <0.05 were termed significant changers. Global analysis of total RPKM datasets to determine overall trends on a gene to gene basis was carried out using R values and distances calculated by Euclidian and Ward methods with the resulting Pearson's correlation scores plotted on a heat map. RPKM values for genes identified as being significantly different between the naïve infected (NI) and preconditioned infected (PI) datasets by Cufflinks were subsequently expressed as a Z-score heatmap with row normalized values. Signatures of expression change were calculated by stratifying the total dataset into groups displaying significant changes (P-value <0.05, 2 fold change) in RPKM score relative to the naïve control (NC) set as follows: up/down infection (altered expression in both naïve and preconditioned infection sets), up/down NI (altered expression only in the naïve infected set), up/down PI (altered expression only in the preconditioned infected set) and up/down preconditioning (altered expression in both the preconditioned naïve and infected states). Go Term analysis was carried out on these gene lists using the David functional annotation tool (https://david.ncifcrf.gov). Analysis of the Hif1α pathway was carried out using KEGG pathway annotations found at the KEGG pathway

database (http://www.genome.jp/kegg/pathway.html). Metabolic gene expression analysis was performed in R on the subset of metabolic genes, defined as the union of genes in KEGG metabolic gene sets and genes of the iSS1393 mouse metabolic reconstruction PMID 23022739. Genes expressed at a level of at least 1 count per million reads in at least three of the samples were filtered out with the EdgeR package PMID 19910308 and differentially expressed genes and their false discovery rate (FDR) corrected p-values were identified by the limma package PMID 25605792. Heatmap analysis was performed using the D3heatmap package and significant clusters were calculated via multiscale bootstrap analysis with the Pvclust package PMID 16595560. For pathway analysis gene expression data was mapped on KEGG metabolic pathways using the Pathview package PMID 23740750 and color-coded according to the directionality of deregulation.

Immunoblot detection of murine leukocyte protein

Murine lysates were prepared by lysis in sodium dodecyl sulfate [SDS]). Immunoblotting was performed with polyclonal anti-mouse HIF-1α (Cell Signaling Technology) primary antibody. Sample loading was confirmed by p38 mitogen-activated protein kinase (MAPK) expression (Cell Signaling Technology). All bands shown were at the predicted molecular weight for the protein of interest.

Seahorse analysis of extracellular acidification

Leukocytes were resuspended in XF assay media at a concentration of $3x10^6$/ml.

Three million cells per condition were plated onto a XF24 cell plate pre-coated with CellTak (Corning, UK). The rate of extracellular acidification (ECAR) was measured at intervals of 7 minutes over a 90 minute cycle using a Seahorse XF24 (Seahorse Bioscience, USA).

Statistical analysis

Data were analysed using Prism 7.0 software (GraphPad Software Inc, San Diego, CA). For comparison of two sample means when cells from the same subject were used, paired *t* tests were performed. Unpiared t tests were used for comparisons between infected normoxic and hypoxic sample means, with one-way ANOVA and Tukey's post-tests used if the comparison also included a vehicle control group. If multiple time points or concentrations were used, repeated measures ANOVA with Dunett's post tests were performed and if comparisons between normoxia and hypoxia or wild type and transgenic mice were required in these experiments, two-way ANOVA with Bonferonni post tests were performed. For bacterial counts, Kruskall-Wallis test with Dunn's multiple comparisons test was used. Survival was analyzed using a log-rank test. Statistical significance was accepted when $p < 0.05$.

Supplementary Materials:

References and Notes

1. H. K. Eltzschig, P. Carmeliet, Hypoxia and inflammation. *N. Engl. J. Med.* **364**, 656-665 (2011).

2. V. A. Kempf, M. Lebiedziejewski, K. Alitalo, J. H. Walzlein, U. Ehehalt, J. Fiebig, S. Huber, B. Schutt, C. A. Sander, S. Muller, G. Grassl, A. S. Yazdi, B. Brehm, I. B. Autenrieth, Activation of hypoxia-inducible factor-1 in bacillary angiomatosis: evidence for a role of hypoxia-inducible factor-1 in bacterial infections. *Circulation* **111**, 1054-1062 (2005).

3. N. Werth, C. Beerlage, C. Rosenberger, A. S. Yazdi, M. Edelmann, A. Amr, W. Bernhardt, C. von Eiff, K. Becker, A. Schafer, A. Peschel, V. A. Kempf, Activation of hypoxia inducible factor 1 is a general phenomenon in infections with human pathogens. *PLoS One* **5**, e11576 (2010).

4. M. A. Matthay, R. L. Zemans, The acute respiratory distress syndrome: pathogenesis and treatment. *Annu. Rev. Pathol.* **6**, 147-163 (2011).

5. R. Hubbard, The burden of lung disease. *Thorax* **61**, 557-558 (2006).

6. C. Alberti, C. Brun-Buisson, S. V. Goodman, D. Guidici, J. Granton, R. Moreno, M. Smithies, O. Thomas, A. Artigas, J. R. Le Gall, G. European Sepsis, Influence of systemic inflammatory response syndrome and sepsis on outcome of critically ill infected patients. *Am. J. Respir. Crit. Care Med.* **168**, 77-84 (2003).

7. T. K. Prajsnar, V. T. Cunliffe, S. J. Foster, S. A. Renshaw, A novel vertebrate model of Staphylococcus aureus infection reveals phagocyte-dependent resistance of zebrafish to non-host specialized pathogens. *Cell. Microbiol.* **10**, 2312-2325 (2008).

8. M. J. Horsburgh, M. O. Clements, H. Crossley, E. Ingham, S. J. Foster, PerR controls oxidative stress resistance and iron storage proteins and is required for virulence in Staphylococcus aureus. *Infect. Immun.* **69**, 3744-3754 (2001).

9. G. P. Bodey, The changing face of febrile neutropenia-from monotherapy to moulds to mucositis. Fever and neutropenia: the early years. *J. Antimicrob. Chemother.* **63 Suppl 1**, i3-13 (2009).

10. I. A. Silver, Tissue PO2 changes in acute inflammation. *Adv. Exp. Med. Biol.* **94**, 769-774 (1977).

11. S. M. Evans, A. E. Schrlau, A. A. Chalian, P. Zhang, C. J. Koch, Oxygen levels in normal and previously irradiated human skin as assessed by EF5 binding. *J. Invest. Dermatol.* **126**, 2596-2606 (2006).

12. D. H. Dockrell, H. M. Marriott, L. R. Prince, V. C. Ridger, P. G. Ince, P. G. Hellewell, M. K. Whyte, Alveolar macrophage apoptosis contributes to pneumococcal clearance in a resolving model of pulmonary infection. *J. Immunol.* **171**, 5380-5388 (2003).

13. M. A. Matthay, G. A. Zimmerman, C. Esmon, J. Bhattacharya, B. Coller, C. M. Doerschuk, J. Floros, M. A. Gimbrone, Jr., E. Hoffman, R. D. Hubmayr, M. Leppert, S. Matalon, R. Munford, P. Parsons, A. S. Slutsky, K. J. Tracey, P. Ward, D. B. Gail, A. L. Harabin, Future research directions in acute lung injury: summary of a National Heart, Lung, and Blood Institute working group. *Am. J. Respir. Crit. Care Med.* **167**, 1027-1035 (2003).

14. C. C. Sheu, M. N. Gong, R. Zhai, E. K. Bajwa, F. Chen, B. T. Thompson, D. C. Christiani, The influence of infection sites on development and mortality of ARDS. *Intensive Care Med.* **36**, 963-970 (2010).

15. Y. Kawakami, F. Kishi, H. Yamamoto, K. Miyamoto, Relation of oxygen delivery, mixed venous oxygenation, and pulmonary hemodynamics to prognosis in chronic obstructive pulmonary disease. *N. Engl. J. Med.* **308**, 1045-1049 (1983).

16. R. Kessler, M. Faller, G. Fourgaut, B. Mennecier, E. Weitzenblum, Predictive factors of hospitalization for acute exacerbation in a series of 64 patients with chronic obstructive pulmonary disease. *Am. J. Respir. Crit. Care Med.* **159**, 158-164 (1999).

17. I. S. Patel, T. A. Seemungal, M. Wilks, S. J. Lloyd-Owen, G. C. Donaldson, J. A. Wedzicha, Relationship between bacterial colonisation and the frequency, character, and severity of COPD exacerbations. *Thorax* **57**, 759-764 (2002).

18. J. D. Tarling, H. S. Lin, S. Hsu, Self-renewal of pulmonary alveolar macrophages: evidence from radiation chimera studies. *J. Leukoc. Biol.* **42**, 443-446 (1987).

19. A. A. Thompson, P. M. Elks, H. M. Marriott, S. Eamsamarng, K. R. Higgins, A. Lewis, L. Williams, S. Parmar, G. Shaw, E. E. McGrath, F. Formenti, F. J. Van Eeden, V. L. Kinnula, C. W. Pugh, I. Sabroe, D. H. Dockrell, E. R. Chilvers, P. A. Robbins, M. J. Percy, M. C. Simon, R. S. Johnson, S. A. Renshaw, M. K. Whyte, S. R. Walmsley, Hypoxia-inducible factor 2alpha regulates key neutrophil functions in humans, mice, and zebrafish. *Blood* **123**, 366-376 (2014).

20. W. G. Kaelin, Jr., P. J. Ratcliffe, Oxygen sensing by metazoans: the central role of the HIF hydroxylase pathway. *Mol. Cell* **30**, 393-402 (2008).

21. T. Cramer, Y. Yamanishi, B. E. Clausen, I. Forster, R. Pawlinski, N. Mackman, V. H. Haase, R. Jaenisch, M. Corr, V. Nizet, G. S. Firestein, H. P. Gerber, N. Ferrara, R. S. Johnson, HIF-1alpha is essential for myeloid cell-mediated inflammation. *Cell* **112**, 645-657 (2003).

22. C. Peyssonnaux, V. Datta, T. Cramer, A. Doedens, E. A. Theodorakis, R. L. Gallo, N. Hurtado-Ziola, V. Nizet, R. S. Johnson, HIF-1alpha expression regulates the bactericidal capacity of phagocytes. *J. Clin. Invest.* **115**, 1806-1815 (2005).

23. S. R. Walmsley, C. Print, N. Farahi, C. Peyssonnaux, R. S. Johnson, T. Cramer, A. Sobolewski, A. M. Condliffe, A. S. Cowburn, N. Johnson, E. R. Chilvers, Hypoxia-induced neutrophil survival is mediated by HIF-1alpha-dependent NF-kappaB activity. *J Exp.Med.* **201**, 105-115 (2005).

24. C. Peyssonnaux, P. Cejudo-Martin, A. Doedens, A. S. Zinkernagel, R. S. Johnson, V. Nizet, Cutting edge: Essential role of hypoxia inducible factor-1alpha in development of lipopolysaccharide-induced sepsis. *J Immunol.* **178**, 7516-7519 (2007).

25. S. R. Walmsley, E. R. Chilvers, A. A. Thompson, K. Vaughan, H. M. Marriott, L. C. Parker, G. Shaw, S. Parmar, M. Schneider, I. Sabroe, D. H. Dockrell, M. Milo, C. T. Taylor, R. S. Johnson, C. W. Pugh, P. J. Ratcliffe, P. H. Maxwell, P. Carmeliet, M. K. Whyte, Prolyl hydroxylase 3 (PHD3) is essential for hypoxic regulation of neutrophilic inflammation in humans and mice. *J. Clin. Invest.* **121**, 1053-1063 (2011).

26. S. R. Walmsley, A. S. Cowburn, M. R. Clatworthy, N. W. Morrell, E. C. Roper, V. Singleton, P. Maxwell, M. K. Whyte, E. R. Chilvers, Neutrophils from patients with heterozygous germline mutations in the von Hippel Lindau protein (pVHL) display delayed apoptosis and enhanced bacterial phagocytosis. *Blood* **108**, 3176-3178 (2006).

27. S. C. Cheng, J. Quintin, R. A. Cramer, K. M. Shepardson, S. Saeed, V. Kumar, E. J. Giamarellos-Bourboulis, J. H. Martens, N. A. Rao, A. Aghajanirefah, G. R. Manjeri, Y. Li, D. C. Ifrim, R. J. Arts, B. M. van der Veer, P. M. Deen, C. Logie, L. A. O'Neill, P. Willems, F. L. van de Veerdonk, J. W. van der Meer, A. Ng, L. A. Joosten, C. Wijmenga, H. G. Stunnenberg, R. J. Xavier, M. G. Netea, mTOR- and HIF-1alpha-mediated aerobic glycolysis as metabolic basis for trained immunity. *Science* **345**, 1250684 (2014).

28. G. M. Tannahill, A. M. Curtis, J. Adamik, E. M. Palsson-McDermott, A. F. McGettrick, G. Goel, C. Frezza, N. J. Bernard, B. Kelly, N. H. Foley, L. Zheng, A. Gardet, Z. Tong, S. S. Jany, S. C. Corr, M. Haneklaus, B. E. Caffrey, K. Pierce, S. Walmsley, F. C. Beasley, E. Cummins, V. Nizet, M. Whyte, C. T. Taylor, H. Lin, S. L. Masters, E. Gottlieb, V. P. Kelly, C. Clish,

P. E. Auron, R. J. Xavier, L. A. O'Neill, Succinate is an inflammatory signal that induces IL-1beta through HIF-1alpha. *Nature* **496**, 238-242 (2013).

29. A. K. Jha, S. C. Huang, A. Sergushichev, V. Lampropoulou, Y. Ivanova, E. Loginicheva, K. Chmielewski, K. M. Stewart, J. Ashall, B. Everts, E. J. Pearce, E. M. Driggers, M. N. Artyomov, Network integration of parallel metabolic and transcriptional data reveals metabolic modules that regulate macrophage polarization. *Immunity* **42**, 419-430 (2015).

30. D. Vats, L. Mukundan, J. I. Odegaard, L. Zhang, K. L. Smith, C. R. Morel, R. A. Wagner, D. R. Greaves, P. J. Murray, A. Chawla, Oxidative metabolism and PGC-1beta attenuate macrophage-mediated inflammation. *Cell Metab.* **4**, 13-24 (2006).

31. P. Levene, G. Meyer, The action of leucocytes on glucose. *J. Biol. Chem* **11**, 361-370 (1912).

32. R. Jones, K. E. McDonald, J. A. Willson, B. Ghesquiere, D. Sammut, E. Daniel, A. J. Harris, A. Lewis, A. A. Thompson, R. S. Dickinson, T. Plant, F. Murphy, P. Sadiku, B. G. Keevil, P. Carmeliet, M. K. Whyte, J. Newell-Price, S. R. Walmsley, Mutations in succinate dehydrogenase B (SDHB) enhance neutrophil survival independent of HIF-1alpha expression. *Blood* **127**, 2641-2644 (2016).

33. B. A. Olenchock, J. Moslehi, A. H. Baik, S. M. Davidson, J. Williams, W. J. Gibson, K. A. Pierce, C. M. Miller, E. A. Hanse, A. Kelekar, L. B. Sullivan, A. J. Wagers, C. B. Clish, M. G. Vander Heiden, W. G. Kaelin, Jr., EGLN1 Inhibition and Rerouting of alpha-Ketoglutarate Suffice for Remote Ischemic Protection. *Cell* **164**, 884-895 (2016).

34. Y. Qiu, K. D. Nguyen, J. I. Odegaard, X. Cui, X. Tian, R. M. Locksley, R. D. Palmiter, A. Chawla, Eosinophils and type 2 cytokine signaling in macrophages orchestrate development of functional beige fat. *Cell* **157**, 1292-1308 (2014).

35. C. C. Blouin, E. L. Page, G. M. Soucy, D. E. Richard, Hypoxic gene activation by lipopolysaccharide in macrophages: implication of hypoxia-inducible factor 1alpha. *Blood* **103**, 1124-1130 (2004).

36. H. Hartmann, H. K. Eltzschig, H. Wurz, K. Hantke, A. Rakin, A. S. Yazdi, G. Matteoli, E. Bohn, I. B. Autenrieth, J. Karhausen, D. Neumann, S. P. Colgan, V. A. Kempf, Hypoxia-independent activation of HIF-1 by enterobacteriaceae and their siderophores. *Gastroenterology* **134**, 756-767 (2008).

37. S. P. Burr, A. S. Costa, G. L. Grice, R. T. Timms, I. T. Lobb, P. Freisinger, R. B. Dodd, G. Dougan, P. J. Lehner, C. Frezza, J. A. Nathan, Mitochondrial Protein Lipoylation and the 2-Oxoglutarate Dehydrogenase

Complex Controls HIF1alpha Stability in Aerobic Conditions. *Cell Metab.* **24**, 740-752 (2016).

38. P. A. Tyrakis, A. Palazon, D. Macias, K. L. Lee, A. T. Phan, P. Velica, J. You, G. S. Chia, J. Sim, A. Doedens, A. Abelanet, C. E. Evans, J. R. Griffiths, L. Poellinger, A. W. Goldrath, R. S. Johnson, S-2-hydroxyglutarate regulates CD8+ T-lymphocyte fate. *Nature* **540**, 236-241 (2016).

39. M. Ko, Y. Huang, A. M. Jankowska, U. J. Pape, M. Tahiliani, H. S. Bandukwala, J. An, E. D. Lamperti, K. P. Koh, R. Ganetzky, X. S. Liu, L. Aravind, S. Agarwal, J. P. Maciejewski, A. Rao, Impaired hydroxylation of 5-methylcytosine in myeloid cancers with mutant TET2. *Nature* **468**, 839-843 (2010).

40. R. Chowdhury, K. K. Yeoh, Y. M. Tian, L. Hillringhaus, E. A. Bagg, N. R. Rose, I. K. Leung, X. S. Li, E. C. Woon, M. Yang, M. A. McDonough, O. N. King, I. J. Clifton, R. J. Klose, T. D. Claridge, P. J. Ratcliffe, C. J. Schofield, A. Kawamura, The oncometabolite 2-hydroxyglutarate inhibits histone lysine demethylases. *EMBO Rep* **12**, 463-469 (2011).

41. C. Lu, P. S. Ward, G. S. Kapoor, D. Rohle, S. Turcan, O. Abdel-Wahab, C. R. Edwards, R. Khanin, M. E. Figueroa, A. Melnick, K. E. Wellen, D. M. O'Rourke, S. L. Berger, T. A. Chan, R. L. Levine, I. K. Mellinghoff, C. B. Thompson, IDH mutation impairs histone demethylation and results in a block to cell differentiation. *Nature* **483**, 474-478 (2012).

42. N. Takeda, E. L. O'Dea, A. Doedens, J. W. Kim, A. Weidemann, C. Stockmann, M. Asagiri, M. C. Simon, A. Hoffmann, R. S. Johnson, Differential activation and antagonistic function of HIF-{alpha} isoforms in macrophages are essential for NO homeostasis. *Genes Dev.* **24**, 491-501 (2010).

43. M. J. Horsburgh, J. L. Aish, I. J. White, L. Shaw, J. K. Lithgow, S. J. Foster, sigmaB modulates virulence determinant expression and stress resistance: characterization of a functional rsbU strain derived from Staphylococcus aureus 8325-4. *J. Bacteriol.* **184**, 5457-5467 (2002).

44. I. Kullik, P. Giachino, T. Fuchs, Deletion of the alternative sigma factor sigmaB in Staphylococcus aureus reveals its function as a global regulator of virulence genes. *J. Bacteriol.* **180**, 4814-4820 (1998).

Acknowledgements:

We thank Dr Lee Murphy for help with the Illumina RNA sequencing.

Funding: This work was supported by Medical Research Council (MRC) Clinical Training Fellowship awards to A.A.R.T (G0802255) and R.S.D (MR/K023845/1), a NIHR Clinical Lectureship and an Academy of Medical Sciences (AMS) starter grant to A.A.R.T., a Wellcome Trust postdoctoral clinical fellowship to A.M. (110086), a Wellcome Trust Senior Clinical Fellowship award to S.R.W. (098516), a Wellcome Trust Senior Clinical Fellowship award to D.H.D. (076945), a British Lung Foundation Fellowship to H.M.M. (F05/7) a Wellcome Trust New Investigator Award to N.M.M. (WT100981MA) and a British Heart Foundation Senior Basic Science Research Fellowship to A.L. (FS/13/48/30453). E.R.C and A.S.C are supported by the NIHR Cambridge Biomedical Research Centre. R.H.S is supported by the MRC. R.R.M. is supported by MRC (MC_PC_U127574433), BBSRC and CEIFC grants. M.M. is supported by the ERC (OxyMO). The MRC / University of Edinburgh Centre for Inflammation Research is supported by an MRC Centre Grant.

Author Contributions:

A.A.R.T., R.S.D., J.P.T., H.M.M., N.M.M., S.J.F, D.H.D., R.S.J., R.R.M., M.K.B.W, and S.R.W. designed the experiments. A.A.R.T., R.S.D., J.P.T., H.M.M.; A.T.; J.W.; L.W., F.M., N.M.M., A. Lewis, N.A., A.M., P.D.S.C., C.D., E.R., E.W., A.G.H., J.A.P., V.F., and A.S.C., performed the experiments. A.A.R.T., R.S.D., J.P.T., H.M.M., S. F., R.H.S., A. Lawrie, M.M., P.S., J.G., F.T., P.C., A.S.C., E.R.C., R.R.M., D.H.D., R.S.J., M.K.B.W., and S.R.W provided technical expertise and performed data analysis. All authors contributed to writing the manuscript.

COMPETING FINANCIAL INTERESTS

The authors declare no competing financial interests.

Fig. 1. Hypoxia induces hypothermia, sickness behavior, cardiac dysfunction and mortality in mice exposed to regional or systemic bacterial infection. (**A-H**) Subcutaneous *S. aureus* infection. Sickness scores (**A**), temperatures (**B**), heart rate (**C**) and systolic blood pressures (**D**) of mice were recorded 12 hours after injection of *S. aureus* or PBS vehicle (Veh) in normoxia (N, 21% O_2) or hypoxia (H, 10% O_2) and after 12 hours in specified oxygen tensions (**G, H**). Echocardiographic measurements of ejection fraction (**E**) and cardiac index (**F**) 12 hours after injection. (**A**) *** P = 0.000044, Normoxia vs. Hypoxia; n = 10; *** P = 0.00005, Hypoxia vs. Vehicle; n = 10 H, 5 Veh; (**B**) *** P = 0.000004, Normoxia vs. Hypoxia; n = 13; *** P = 0.00001, Hypoxia vs. Vehicle; n = 13 H, 5 Veh; one-way ANOVA with Tukey's post-tests. (**C**) * P = 0.0186, N vs. H; n = 5; * P = 0.0151, H vs. Veh H; n = 5 H, 3 Veh H; unpaired t tests. (**E**) *** P = 0.000753, N vs. H; n = 4; (**F**) * P = 0.0298, N vs. H; n = 4; one-way ANOVA with Tukey's post-tests. (**G**) *** P = 0.000003, 21% vs. 10%; *** P = 0.000036, 15% vs. 10%; ** P = 0.00217, 12% vs. 10%; (**H**) *** P = 0.000005, 21% vs. 10%; *** P = 0.000004, 15% vs. 10%; ** P = 0.00109, 12% vs. 10%; 21% n = 9, 15% n = 5, 12% n = 5; 10% n= 9; one-way ANOVA with Tukey's post-tests.(**I-Q**) Intra-tracheal *S. pneumoniae*. Sickness scores (**I**) and temperatures (**J**) of mice 14h and 24h after intratracheal instillation of 10^7 cfu of *S. pneumoniae* D39 or vehicle (V) and housed in normoxia (N, 21% O_2) or hypoxia (H, 10% O_2). (**I**) * P = 0.0282, 14h N vs. H; n = 21 N, 15 H; (**J**) * P = 0.0459, 14h N vs. H; n = 21 N, 15 H; *** P = 0.000036, 24h N vs. H; n = 8; one-way ANOVA with Tukey's post-tests. (**K, L)** Viable bacterial counts recovered from homogenized lung (**K**) or whole blood (**L**) at 14h or 24h after instillation of *S. pneumoniae* in specified oxygen tension. (**L**) * P = 0.0239, 14h N vs. H; n = 21 N, 15 H; Kruskal-Wallis with Dunn's post-test comparisons. Total

bronchoalveolar lavage (BAL) cell counts (**M**) and neutrophil (**N**) and macrophage (**O**) counts at 14h or 24h post instillation of *S. pneumoniae* or vehicle in specified oxygen tension. (**M**) ** $P = 0.0034$, 14h N vs. H; n = 21 N, 15 H; unpaired t-test. (**N**) ** $P = 0.01$, 14h N vs. H; n = 21 N, 15 H; unpaired t-test; (**O**) * $P = 0.0172$, 14h N vs. H; n = 21 N, 15 H; unpaired t-test. (**P**) BAL supernatant IgM concentration in normoxia (N) and hypoxia (H) 14h and 24h after instillation. (**Q**) Kaplan Meier survival curves of mice instilled with *S. pneumoniae* and housed in normoxia or hypoxia. (**Q**) *** $P = 0.0002$ N vs. H; n = 10; log-rank test. Horizontal lines (**A-B, G-H, I-O**) or bars (**C-F, P**) are mean +/- SEM.

Fig. 2. Hypoxic preconditioning confers protection from hypothermia and sickness behavior and reverses the negative energy balance observed with infection in the setting of hypoxia.

(**A-B**) Subcutaneous *S. aureus*. Mice were preconditioned in hypoxia for 7 days then challenged with subcutaneous SH1000 and sickness scores (**A**) and temperatures (**B**) recorded after 12 hours. (**A**) * $P = 0.0365$ Hypoxia vs. Preconditioned; n = 7; (**B**) ** $P = 0.00855$ Hypoxia vs. Preconditioned; n = 7; unpaired t-tests. (**C-P**) Intra-tracheal *S. pneumoniae*. Mice were instilled with PBS control (Veh) or *S. pneumoniae* (Spn) and housed in normoxia (N), hypoxia (H) or in hypoxia following preconditioning (Pre H). Sickness scores (**C**) and temperatures (**D**) were recorded at 14 hours, and Kaplan Meier survival curves performed over a 168-hour period (**E**). (**C**) ** $P = 0.00114$, Spn N vs. Spn H; ** $P = 0.00114$, Spn H vs. Spn Pre H; (**D**) * $P = 0.00779$, Spn N vs. Spn H; *** $P = 0.0006$, Spn H vs. Spn Pre H; n = 6 Spn N, 5 Spn H, 6 Spn Pre H; one-way ANOVA with Tukey's post-tests; (**E**)

P = 0.0005, Normoxia vs. Hypoxia, *P* = 0.000012 Hypoxia vs. Pre H; n = 10; Log-rank test. **(F)** Respiratory exchange ratios were calculated from indirect calorimetric analysis undertaken over a 1 hour period following a 20 hour exposure to *S. pneumoniae*. * *P* = 0.0230, N vs. H; * *P* = 0.0181, H vs. Pre H; n = 4; one-way ANOVA with Tukey's post-test. Separately, 24 hours following infection, livers were harvested and PAS stained for glycogen (**G**), inguinal (**H**) and intrascapular (**I**) fat reserves measured by weight, serum β-hydroxybutyrate levels quantified (**J**) and blood glucose levels determined relative to survival outcome (**K**). For accurate glucose monitoring, a sub group of mice were fasted for the last 6 hours of experimental procedure and paired glucose (**L**) and insulin (**M**) levels recorded. (**H**) * *P* = 0.0429, Spn N vs. Spn H; * *P* = 0.0467, Spn H vs. Veh H; * *P* = 0.0208, Spn Pre H vs. Veh Pre H; n = 4; (**I**) ** *P* = 0.0041, Spn N vs. Spn H; ** *P* = 0.0078, Spn H vs. Spn Pre H; * *P* = 0.0219, Veh N vs. Veh H; n = 4; (**J**) * *P* = 0.0165 Spn N vs. Spn H, *** *P* = 0.000083, Spn H vs. Spn Pre H; n = 4; one-way ANOVA with Tukey's post-tests. (**K**) **** *P* < 0.000001, survived (n = 25) vs. culled (n = 24); unpaired t-test. (**L**) * *P* = 0.0101, N vs. H; * *P* = 0.0298, H vs. Pre H; n = 12 N, 9 H, 9 Pre H; unpaired t-tests; (**M**) * *P* = 0.0106, N vs. H; n = 12 N, 9 H; unpaired t-test. In a separate group of animals, ^{18}F-FDG was administered 5 hours (**N**) and 23 hours following instillation of *S. pneumoniae* (SPn) (**O**, **P**). Radioactivity levels were assessed with a gamma counter on brown fat (**N**) and hearts (**P**) and in vivo standardized glucose uptake values determined by positron emission tomography (PET) (**O**). (**N**) * *P* = 0.0177, Spn N vs. Spn H; * *P* = 0.0185, Spn H vs. Spn Pre H; n = 4 Spn N, 4 Spn H, 3 Spn Pre H; one-way ANOVA with Tukey's post-test. (**P**) * *P* = 0.0307, Spn N vs. Spn Pre H; * *P* = 0.0237, Spn H vs. Spn Pre H; n = 3 Spn N, 4

Spn H, 4 Spn Pre H; one-way ANOVA with Tukey's post-test. (**Q, R**) Subcutaneous *S. aureus*. Echocardiographic measurements of ejection fraction (**Q**) and cardiac index (**R**) were undertaken 12 hours after injection of *S. aureus* in normoxia (N), hypoxia (H) or in hypoxia following preconditioning (Pre H). (**Q**) *** $P = 0.000485$, N vs. H; n = 4 N, 6 H; * $P = 0.0132$, H vs. Pre H; n = 6; (**R**) ** $P = 0.00133$, N vs. H; n = 4 N, 6 H; *** $P = 0.00041$, H vs. Pre H; n = 6; one-way ANOVA with Tukey post-tests. Horizontal lines (**A-D, N, P**) or bars (**F, H-M, Q, R**) are mean +/- SEM.

Fig. 3. Hypoxic preconditioning confers long-term protection from adverse responses to infection in hypoxia and changes the transcriptome of circulating leukocytes.

(**A-D**) Duration of preconditioning effect. Mice were preconditioned in hypoxia for 7 days, SH1000 injected subcutaneously after either 7 days (**A, B**) or 28 days (**C, D**) back in normoxia and sickness scores (**A, C**) and temperatures (**B, D**) recorded after a further 12 hours. (**B**) * $P = 0.0203$; n = 5; (**C**) * $P = 0.0142$; n = 6 H, 7 Pre H; (**D**) * $P = 0.0238$; n = 6 H, 7 Pre H; unpaired t-tests. (**E-G**) Bone marrow transfer. Mice were preconditioned in hypoxia for 7 days, bone marrow harvested and injected into wildtype C57BL/6 mice pre-irradiated with 12 fractions of 1Gy (Pre H to WT), with non-preconditioned mice used as marrow donor controls (Un to WT). Following 3 weeks re-constitution mice were challenged either with subcutaneous SH1000 in hypoxia (**E, F**) or intra-tracheal *S. pneumoniae* (**G**). Sickness scores (**E**) and temperature (**F**) were recorded after 12 hours. (**E**) * $P = 0.0444$ Pre H to WT vs. Un to WT; n = 6 Pre H to WT, 5 Un to WT; unpaired t-test. (**G**) Kaplan Meier survival

curves were undertaken of mice instilled with *S. pneumoniae* and housed in normoxia or hypoxia. *** $P = 0.0007$, Normoxia vs. Hypoxia; * $P = 0.0305$, Naive BM hypoxia vs. Pre BM hypoxia; n = 8; log-rank test. (**H**) Myeloid cell depletion. 12 hours following injection with vehicle control (PBS), anti-Ly6G antibody (Ly6G), clodronate (Clod) or control liposomes containing PBS (Lipo), animals were challenged with subcutaneous SH1000 and rectal temperatures measured after 12 hours. **** $P = 0.00000002$, Normoxia PBS vs. Hypoxia PBS; * $P = 0.0235$ Hypoxia PBS vs. Hypoxia Ly6G; * $P = 0.0146$, Hypoxia Ly6G vs. Hypoxia Clod; n = 8 N PBS, 7 H PBS, 7 N Ly6G, 7 H Ly6G, 8 N Clod, 8 H Clod, 3 N Lipo, 3 H Lipo; 2-way ANOVA with Tukey's post-test. Horizontal lines (**A-F, H**) are mean +/- SEM. **(I-K)** RNA-seq. Blood leukocytes were harvested from hypoxia naïve mice instilled with *S. pneumoniae* in 10% O_2 (naïve infected, NI) or vehicle control (naïve control, NC) or following hypoxic preconditioning (preconditioned infected, PI and preconditioned control, PC). (**I**) Pearson correlation heatmap analysis with hierarchical clustering on total RNA-seq datasets. Pearson correlation scores are plotted from 0 (white) to 1(dark blue) in steps of 0.1. (**J**) Heatmap of column normalized Z-scores for each gene identified as changing significantly between the naïve infected and preconditioned infected samples. Blue: Z-score -2, Yellow: Z-score +2. (**K**) Signatures of differential gene expression across the datasets. Genes were selected based on fold change values >2 fold induced or repressed relative to naïve control expression status (=1). Numbers of genes per group are shown in square brackets above the plots.

Fig. 4. Repression of leukocyte HIF-1α suppresses glucose utilization resulting in phenotypic rescue.

(**A-C**) HIF-1 expression. Leukocytes were harvested from mice injected with SH1000 (**A)** or *S. pneumoniae* (Spn) (**B, C**) in normoxia (N, 21% O_2), hypoxia (H, 10% O_2) or in hypoxia following hypoxic pre-conditioning (Pre H). RNA and protein were extracted and relative expression of *Hif1a* and *Hif1b* RNA normalized to *Actb* (**A, B**) with protein to P38 (**C**). (**B**) *Hif1a* * P = 0.0447, H vs. Pre H; n = 6 N, 7 H, 6 Pre H; unpaired t-test; *Hif1b* * P = 0.0272, H vs. Pre H; n = 6 N, 7 H, 6 Pre H; unpaired t-test. (**D-E**) Metabolic gene expression analysis. Correlation heatmap and hierarchical clustering analysis was undertaken of metabolic transcripts identified within the RNA-seq dataset of blood leukocytes harvested 14 hours after intra-tracheal installation of *S. pneumoniae* (Spn) in normoxia (N), hypoxia (H) or in hypoxia following preconditioning (Pre H). Color scale: red, higher correlation; blue, lower correlation, with significance determined by multi-scale bootstrap analysis (P<0.01) and represented by changes in color within the dendrogram (**D**). The log fold change of individual glycolytic enzyme transcripts was determined for preconditioned leukocytes relative to naïve controls (green: upregulated by at least by 60 %; orange: downregulated by 60%) (**E**). Changes in transcript abundance were further validated in the SH1000 model by real time PCR (**E**). (**E**) *Glut1* * P = 0.0168, N vs. H; ** P = 0.0082, H vs. Pre H; *Tpi1* ** P = 0.0074, N vs. H; *Gapdh* ** P = 0.0015, N vs. H; * P = 0.0345, H vs. Pre H; *Pkm* * P = 0.0460, H vs. Pre H; n = 6 N, 6 H, 5 Pre H; one-way ANOVA with Tukey's post-tests. (**F-H**) Functional changes in metabolism. (**F**) Leukocytes were harvested from mice challenged with subcutaneous PBS or SH1000 and housed in normoxia (N), hypoxia (H) or in

hypoxia following preconditioning (Pre H). Glycolytic rates following infection were indirectly measured by extracellular acidification rates (ECAR) relative to vehicle controls. *** $P = 0.0007$, N vs. H; * $P = 0.0466$, N vs. Pre H; * $P = 0.0114$, H vs. Pre H; n = 3, one-way ANOVA with Tukey's post test. (**G-H**) ^{18}F-FDG was administered 5 hours following instillation of *S. pneumoniae* (Spn) and radioactivity levels in harvested blood leukocytes (**G**) and bronchoalveolar lavage (BAL) cells (**H**) assessed after 1 hour by gamma counts. (**G**) * $P = 0.0269$, H vs. Pre H; n = 4 N, 3 H, 4 Pre H; (**H**) * $P = 0.0124$, H vs. Pre H, n = 3 N, 4 H, 4 Pre H; one-way ANOVA with Tukey's post-tests. (**I-K**) Myeloid loss of HIF-1α. Sickness scores (**I**) and rectal temperatures (**J**) were determined in wild-type C57BL/6 (WT) and *Hif1a*$^{flox/flox}$;*LysMCre*$^{+/-}$ (*Hif1a*$^{-/-}$) mice 12 hours following subcutaneous injection of SH1000. (**I**) ** $P = 0.00144$ WT H vs. *Hif1a*$^{-/-}$ H; n = 8 WT H, 10 *Hif1a*$^{-/-}$ H; (**J**) *** $P = 0.000545$ WT H vs. *Hif1a*$^{-/-}$ H; n = 7 WT H, 10 *Hif1a*$^{-/-}$ H; 2-way ANOVA with Tukey's post-tests. (**K**) In a separate group of animals random glucose levels were measured in wild-type (WT) and *Hif1a*$^{flox/flox}$;*LysMCre*$^{+/-}$ (*Hif1a*$^{-/-}$) mice 20 hours following infection with S. pneumonia in 10% O_2. * $P = 0.0158$, WT vs. *Hif1a*$^{-/-}$; n = 21 WT, 23 *Hif1a*$^{-/-}$; unpaired t-test.

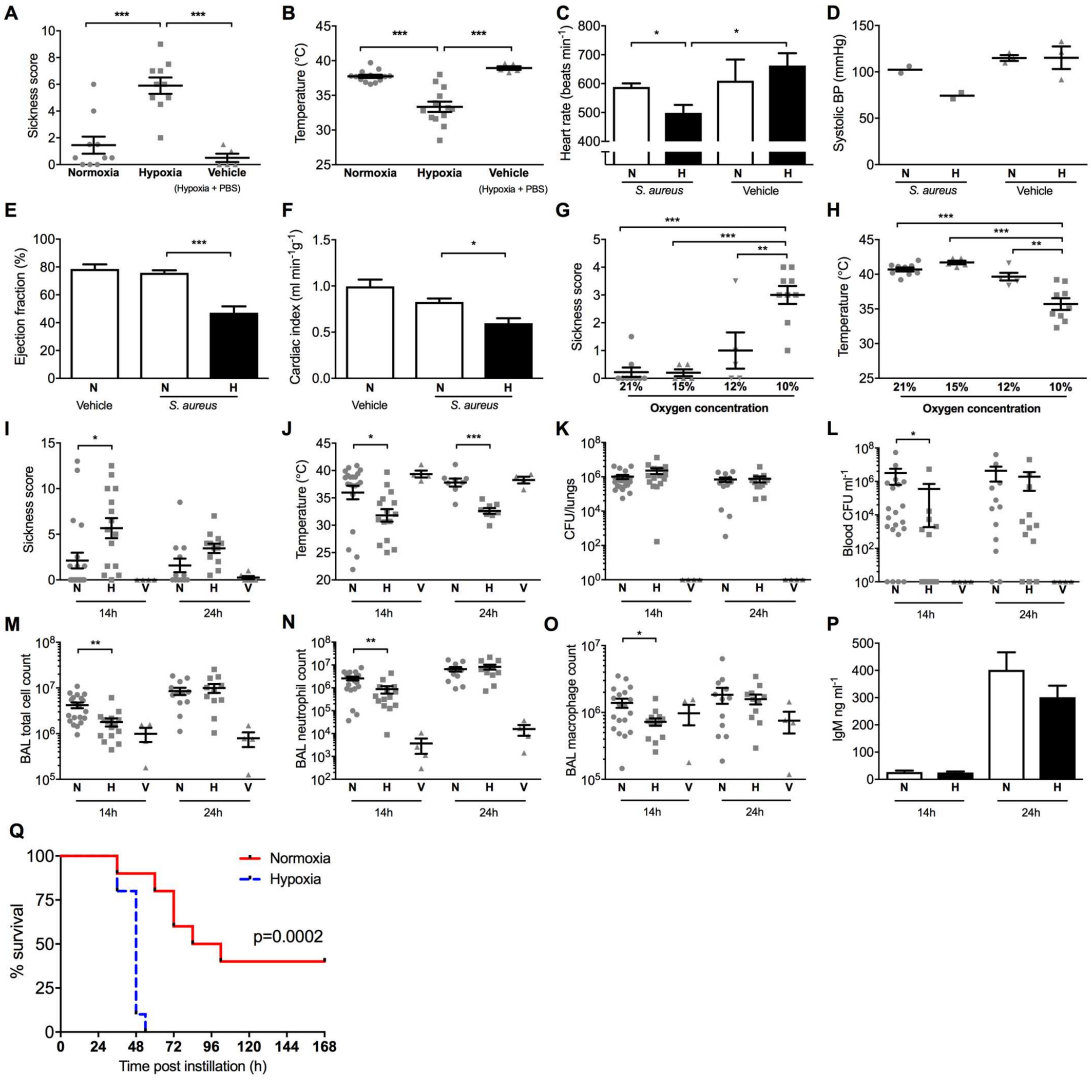
A
Sickness score
Normoxia
Hypoxia
Vehicle
(Hypoxia + PBS)
B
Temperature (°C)
C
Heart rate (beats min-1)
S. aureus
Vehicle
D
Systolic BP (mmHg)
E
Ejection fraction (%)
F
Cardiac index (ml min-1 g-1)
G
Sickness score
Oxygen concentration
H
Temperature (°C)
I
Sickness score
J
Temperature (°C)
K
CFU/lungs
L
Blood CFU ml-1
M
BAL total cell count
N
BAL neutrophil count
O
BAL macrophage count
P
IgM ng ml-1
14h
24h
Q
Normoxia
Hypoxia
p=0.0002
% survival
Time post instillation (h)

Fig. 1

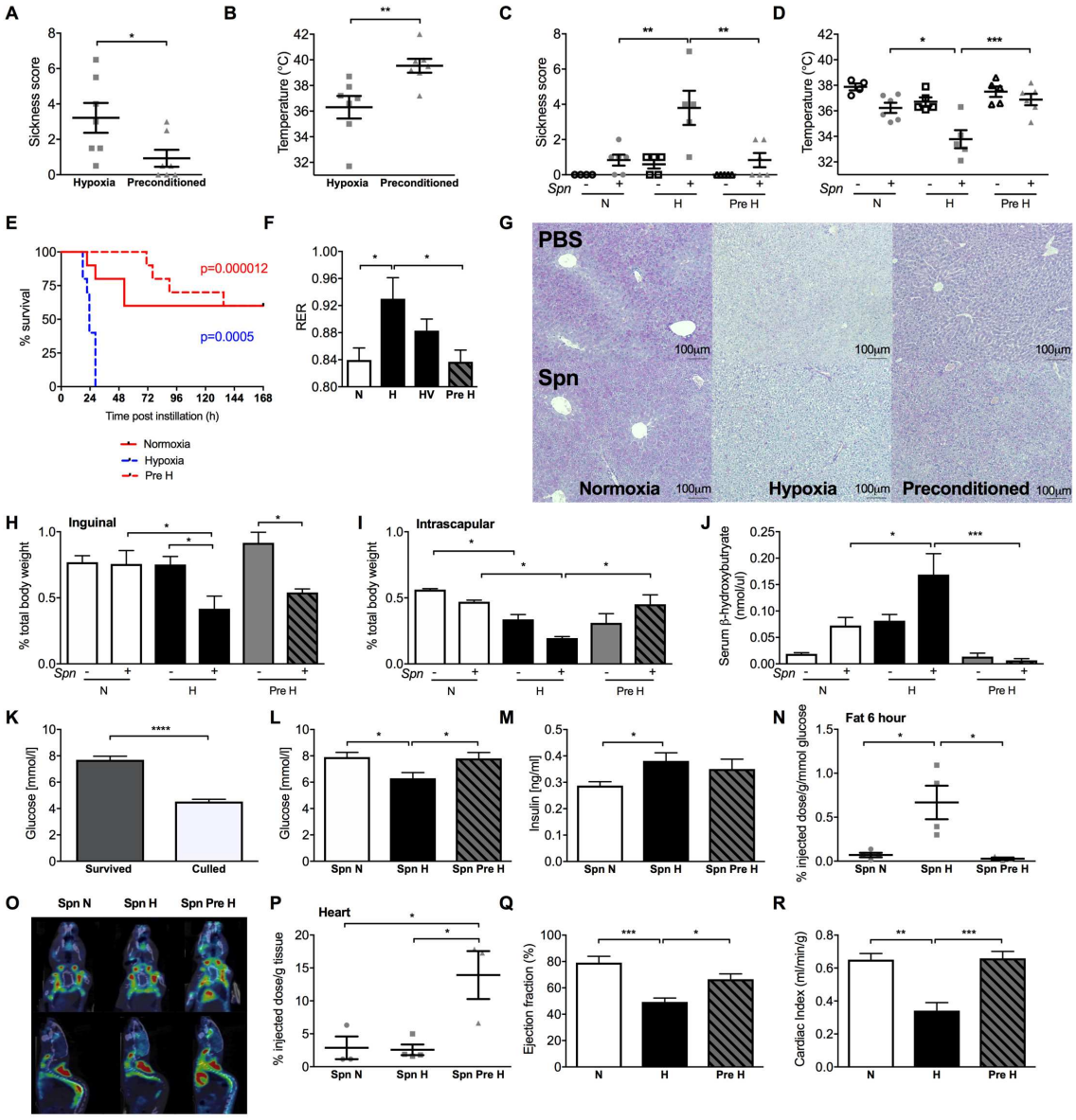
A
Sickness score
Hypoxia
Preconditioned
B
Temperature (°C)
Hypoxia
Preconditioned
C
Sickness score
Spn
N
H
Pre H
D
Temperature (°C)
Spn
N
H
Pre H
E
% survival
p=0.000012
p=0.0005
Time post instillation (h)
Normoxia
Hypoxia
Pre H
F
RER
N
H
HV
Pre H
G
PBS
Spn
Normoxia
Hypoxia
Preconditioned
100µm
H
Inguinal
% total body weight
I
Intrascapular
% total body weight
J
Serum β-hydroxybutryate (nmol/ul)
K
Glucose [mmol/l]
Survived
Culled
L
Glucose [mmol/l]
Spn N
Spn H
Spn Pre H
M
Insulin [ng/ml]
N
Fat 6 hour
% injected dose/g/mmol glucose
O
Spn N
Spn H
Spn Pre H
P
Heart
% injected dose/g tissue
Q
Ejection fraction (%)
R
Cardiac Index (ml/min/g)

Fig. 2

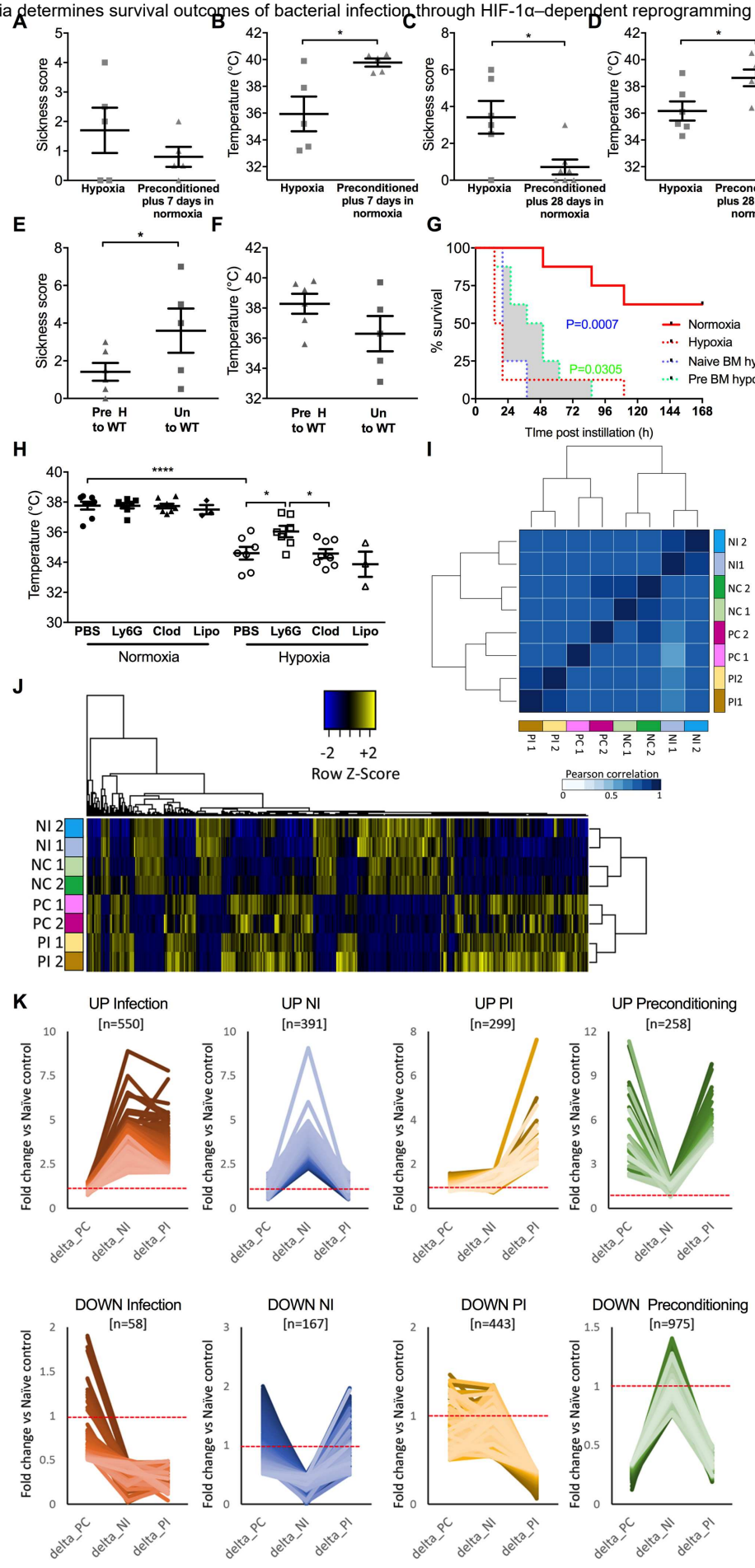
A
Sickness score
Hypoxia
Preconditioned plus 7 days in normoxia
B
Temperature (°C)
Hypoxia
Preconditioned plus 7 days in normoxia
C
Sickness score
Hypoxia
Preconditioned plus 28 days in normoxia
D
Temperature (°C)
Hypoxia
Preconditioned plus 28 days in normoxia
E
Sickness score
Pre H to WT
Un to WT
F
Temperature (°C)
Pre H to WT
Un to WT
G
% survival
P=0.0007
P=0.0305
Normoxia
Hypoxia
Naive BM hypoxia
Pre BM hypoxia
TIme post instillation (h)
H
Temperature (°C)
PBS Ly6G Clod Lipo PBS Ly6G Clod Lipo
Normoxia
Hypoxia
I
NI 2
NI1
NC 2
NC 1
PC 2
PC 1
PI2
PI1
Pearson correlation
J
-2 +2
Row Z-Score
NI 2
NI 1
NC 1
NC 2
PC 1
PC 2
PI 1
PI 2
K
UP Infection [n=550]
UP NI [n=391]
UP PI [n=299]
UP Preconditioning [n=258]
DOWN Infection [n=58]
DOWN NI [n=167]
DOWN PI [n=443]
DOWN Preconditioning [n=975]
Fold change vs Naïve control
delta_PC
delta_NI
delta_PI

Fig. 3

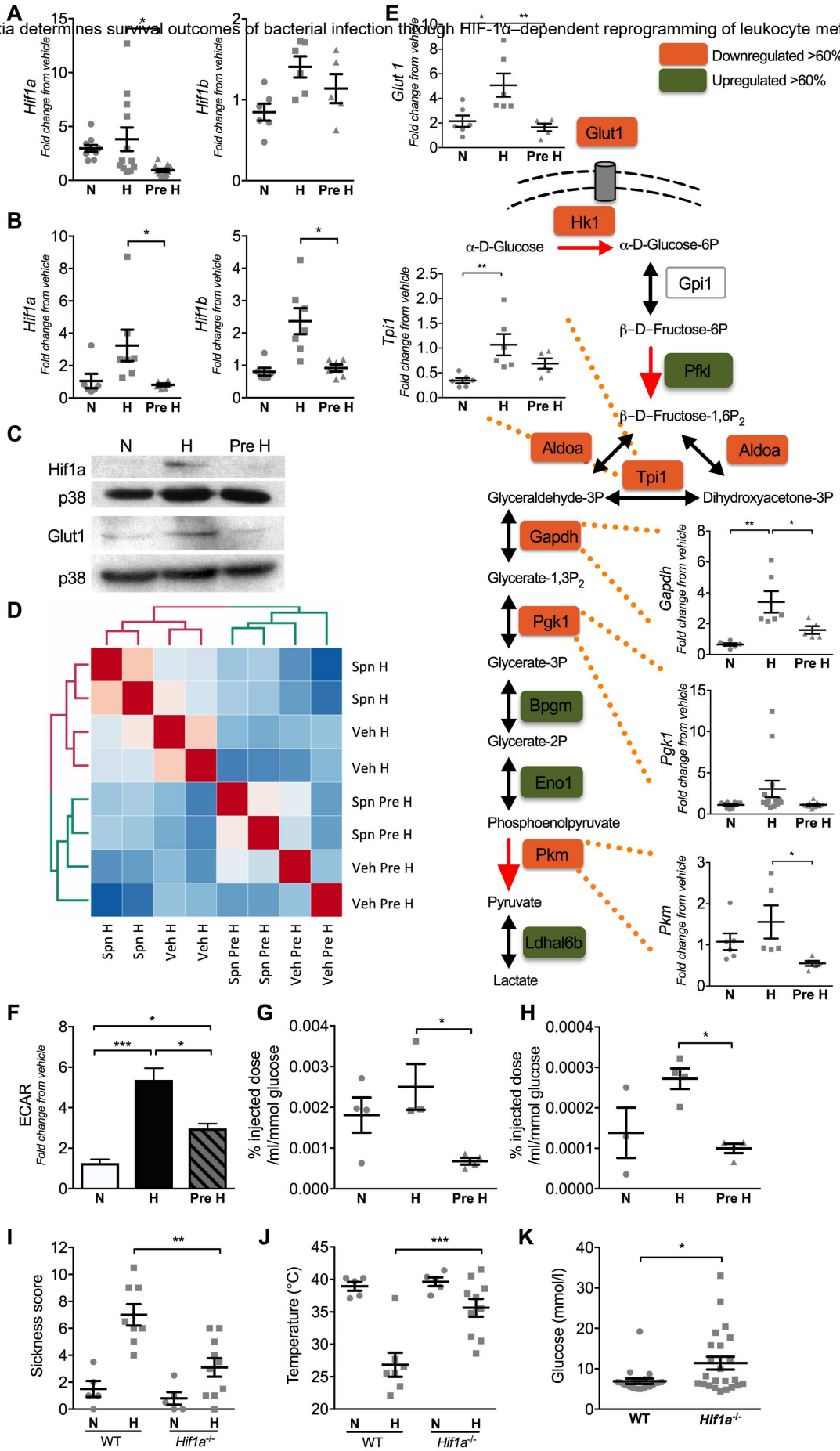
A
Hif1a
Fold change from vehicle
Hif1b
Fold change from vehicle
N
H
Pre H
B
Hif1a
Hif1b
C
N
H
Pre H
Hif1a
p38
Glut1
p38
D
Spn H
Spn H
Veh H
Veh H
Spn Pre H
Spn Pre H
Veh Pre H
Veh Pre H
E
Glut 1
Downregulated >60%
Upregulated >60%
Glut1
Hk1
α-D-Glucose
α-D-Glucose-6P
Gpi1
Tpi1
β-D-Fructose-6P
Pfkl
β-D-Fructose-1,6P2
Aldoa
Aldoa
Tpi1
Glyceraldehyde-3P
Dihydroxyacetone-3P
Gapdh
Glycerate-1,3P2
Pgk1
Glycerate-3P
Bpgm
Glycerate-2P
Eno1
Phosphoenolpyruvate
Pkm
Pyruvate
Ldhal6b
Lactate
Gapdh
Pgk1
Pkm
F
ECAR
Fold change from vehicle
G
% injected dose /ml/mmol glucose
H
% injected dose /ml/mmol glucose
I
Sickness score
WT
Hif1a-/-
J
Temperature (°C)
WT
Hif1a-/-
K
Glucose (mmol/l)
WT
Hif1a-/-

Fig. 4